ASTR 7500: Solar & Stellar Magnetism

Hale CGEP Solar & Space Physics

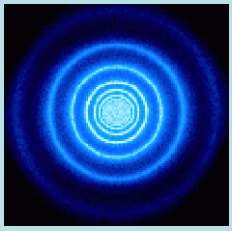

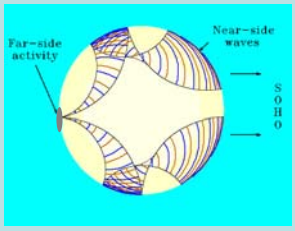

Profs. Brad Hindman & Juri Toomre

Lecture 24 Thurs 18 Apr 2013

zeus.colorado.edu/astr7500-toomre

Lecture 24 Helioseismic Discoveries

- Results from Global Helioseismology
  - Sound speed and density inversions
  - Rotation rate inversion
- Local Helioseismology
  - Ring analysis
  - Meridional Flows
  - Flows around active regions and sunspots
  - Farside imaging

Results from Global Helioseismology

Internal Thermodynamics

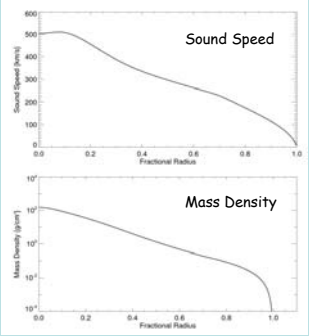

Solar model and an inversion from observations

Since the solar model used in the inversion is very good (predicts frequencies to within a percent or so of the observed), the inversion results and the model are indistinguishable in plots of this nature.

Closer Look

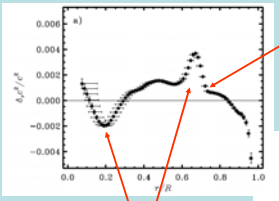

Bottom of the convection zone

Error

Depth Resolution

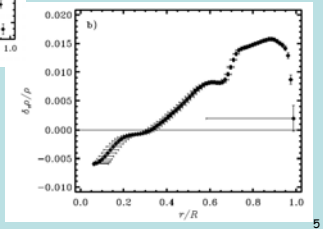

Likely due to weak mixing of elements (or perhaps errors in the model opacity).

Overlapping Kernels

$$\delta\omega_{ln}^2 = \int \mathcal{K}_{ln}(r)\frac{\delta c^2}{\tilde{c}^2}\,dr$$

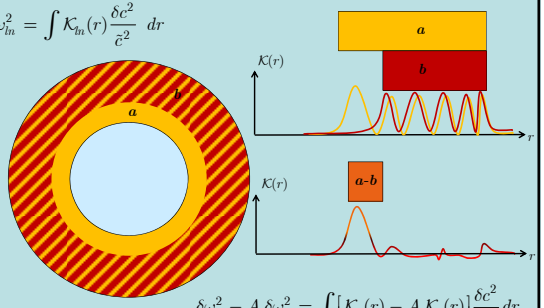

$$\delta\omega_a^2 - A_b\delta\omega_b^2 = \int \left[\mathcal{K}_a(r) - A_b\mathcal{K}_b(r)\right]\frac{\delta c^2}{\tilde{c}^2}\,dr$$

Solar Rotation

Remember that that the eigenfrequencies were degenerate in the quantum number m, for a spherically symmetric star. Rotation breaks that degeneracy.

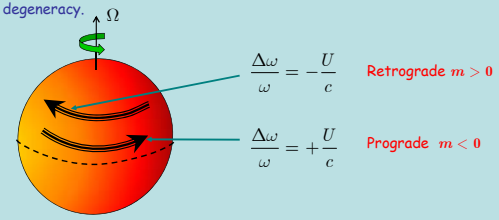

$$W(r)\ Y_l^m(\theta,\varphi)\ e^{-i\omega t} \sim W(r)\ P_l^m(\cos\theta)\ e^{i(m\varphi-\omega t)}$$

7

Differential Rotation

Rotation causes a splitting of the frequency that varies with m. As before, the splitting can be expressed using a kernel

$$\omega_{nlm} - \omega_{nl0} = \Delta\omega_{nlm} = m\iint \mathcal{K}_{n,\Omega}(r,\theta)\ \Omega(r,\theta)\ r dr\, d\theta$$

no φ?

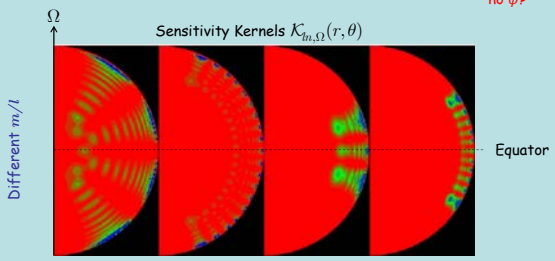

8

Inversion for Rotation

$$\omega_{nlm} - \omega_{nl0} = \Delta\omega_{nlm} = m\iint \mathcal{K}_{n,\Omega}(r,\theta)\ \Omega(r,\theta)\ r dr\, d\theta$$

An inversion for the rotation rate proceeds just as for the sound speed. We parameterize the rotation rate with a set of free parameters α_j.

$$\Omega(r,\theta) \approx \Omega_{\rm mod}(r,\theta;\boldsymbol{\alpha})$$

We find the parameters α_j that best fit the data by minimizing . . .

$$\chi^2(\boldsymbol{\alpha}) = \sum_{nlm} \frac{\left[\Delta\omega_{nlm} - m\iint \mathcal{K}_{n,\Omega}(r,\theta)\ \Omega_{\rm mod}(r,\theta;\boldsymbol{\alpha})\ r dr\, d\theta\right]^2}{\sigma_{nlm}^2} + \lambda\iint \left|\nabla^2\Omega_{\rm mod}(r,\theta;\boldsymbol{\alpha})\right|^2 r dr\, d\theta$$

9

Differential Rotation in the Sun

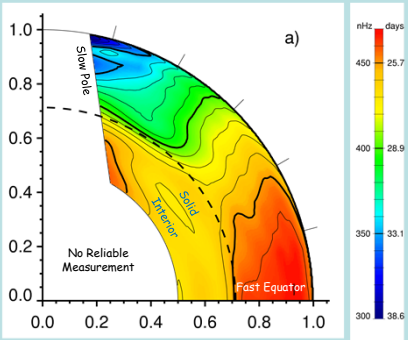

MDI data

10

Shear Layers

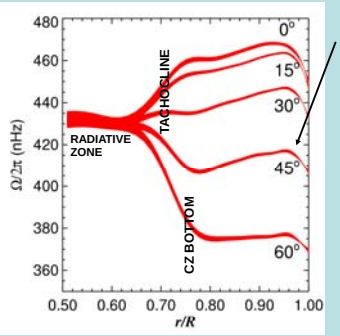

NEAR-SURFACE SHEAR LAYER

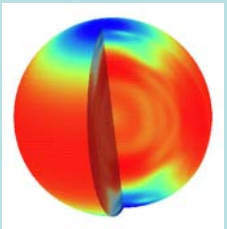

11

Meridional Circulation

Flux Transport Dynamos

- Carries the poloidal flux from the surface to the tachocline.
- Sets the period of the activity cycle.

Miesch et al. 2008

Numerical Simulations

- Helioseismic constraints on the differential rotation have been invaluable guides.
- Meridional circulations could do the same.

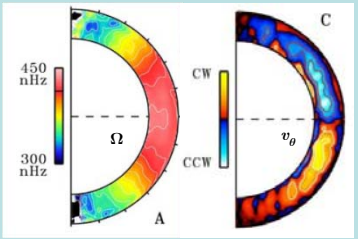

Bah!

Unfortunately, the *global modes* are insensitive to a meridional flow.

Why?

- The global modes are standing waves in latitude (unlike in longitude)
- They spend an equal amount of time swimming upstream and downstream.

$$W(r)\ P_l^m(\cos\theta)\ e^{i(m\varphi-\omega t)}$$

Real function (standing wave) — Complex (propagating)

The global modes also have the weakness that their energy densities (or the sensitivity kernels) are:

- Symmetric about the equator (insensitive to hemispheric differences)
- Constant with longitude (insensitive to longitudinal variation)

$$\left[W(r)\ P_l^m(\cos\theta)\right]^2 \quad \left|e^{i(m\varphi-\omega t)}\right|^2 = 1$$

Local Helioseismology

Peaks to Ridges

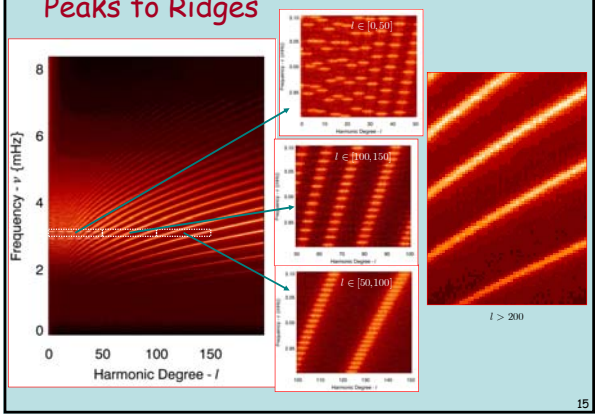

Wavenumber Regimes

Low-degree waves ($l < 200$)

- Weakly damped and able to circumnavigate the sun.
- Form resonances → integer l
- Isolated peaks
- The frequencies are global measures of the internal properties
- Used by Global Helioseismology

High-degree waves ($l > 200$)

- Highly damped and unable to travel completely around the sun.
- All horizontal wavenumbers are allowed
- Ridges of merges peaks
- The frequencies are local measures of the internal properties
- Used by Local Helioseismology

Two Primary Flavors

Local helioseismology utilizes the high-degree waves to make local estimates of solar properties. There are two primary flavors (some with nuts, others with chocolate chips, etc.)

Correlation Procedures

(*Time-Distance Tomography, Acoustic Holography*)

- The fundamental measurement is the time it takes a signal to travel from one point on the surface to a second point.
- Such measurements are made by cross-correlating the two time series associated with those points and fitting for the time lag associated with maximum correlation.

Spectral Procedures

(*Ring Analysis, Fourier-Hankel Decomposition*)

- The fundamental measurement is the frequencies of local modes.
- Such measurements are made by fitting peaks in a power spectrum..

Ring Analysis

Plane Wave Decomposition

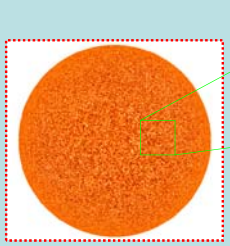

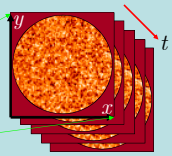

Each image is apodized and then transformed

$$v(k_x, k_y, \omega) = \iiint e^{-i\vec{k}_h \cdot \vec{x}} e^{i\omega t} v_{los}(x, y, t)$$

Why plane waves?
Waves of short wavelength (larger wavenumber) are confined near the surface.

19

Ring Spectra

Power $= \left| v(k_x, k_y, \omega) \right|^2$

Since there are two spatial dimensions (x, y) and the time dimension t, the spectra are 3D.

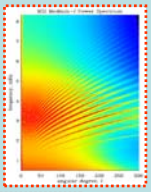

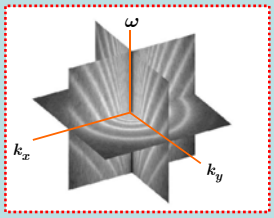

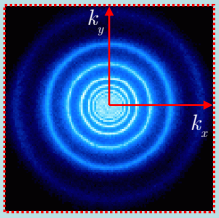

Local Spectra

20

Rings!

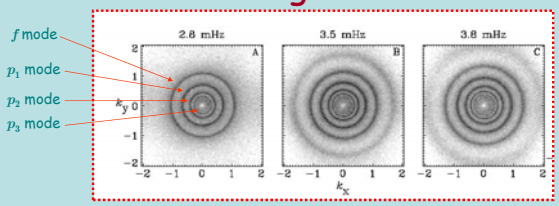

The modes appear as nested trumpets aligned with the frequency axis.

Cuts at constant frequency produce nested rings that have larger radii for larger frequencies.

Changes in the mode frequencies manifest as changes to the radii of the rings. Therefore, careful measurement of the radii can be used to determine subsurface structure (c^2, ρ, etc.).

21

The effects of a wind

In a 2-D homogeneous fluid with sound speed c, the dispersion relation for acoustic waves is,

$$\omega^2 = k^2 c^2 = (k_x^2 + k_y^2)c^2$$

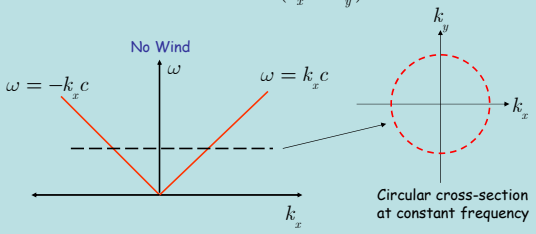

Circular cross-section at constant frequency

22

Doppler Shift Caused by a Wind

A wind with speed U in the x direction causes a Doppler shift. The shift can be expressed using a Galilean transformation

$$\left(\omega - k_x U\right)^2 = k^2 c^2$$

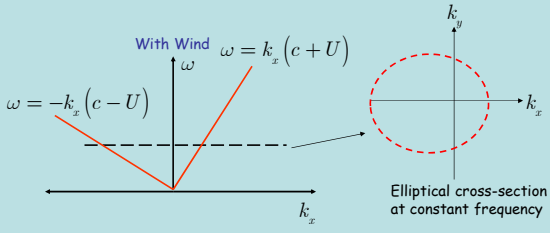

Elliptical cross-section at constant frequency

23

Effect on p-Mode Spectra

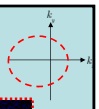

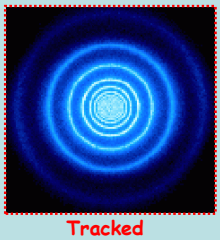

Tracked

The above spectra was obtained by following the same patch of fluid as it rotates across the solar disk. This removes the large rotational velocity.

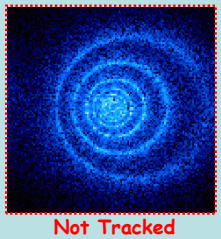

Not Tracked

The above spectra was obtained by studying the same area on the solar disk. Equatorial rotation results in a speed of ~ 2000 m/s.

24

Measuring Frequencies and Doppler Shifts

The frequency of a mode and its Doppler shift are determined by fitting the spectra with a "line profile", usually a Lorentzian function of frequency. This fitting is performed for each value of k_h in the spectra.

$$P(\vec{k}_h,\omega) = \frac{A}{\left(\omega - \omega_n + \vec{k}_h \cdot \vec{U}\right)^2 + \Gamma^2}$$

$$\vec{U} = U_x\hat{x} + U_y\hat{y}$$

A - Amplitude
Γ - Line widths
U_x and U_y - Doppler shifts
ω_n - Mode frequency

The frequencies ω_n are a measure of the sound speed below the surface.

The Doppler shifts U_x and U_y measure the flow speed in the x and y directions.

Building up a map

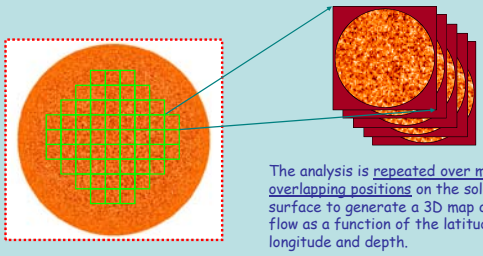

The analysis is repeated over many overlapping positions on the solar surface to generate a 3D map of the flow as a function of the latitude, longitude and depth.

The analysis is repeated on a daily basis to build up a time series of 3D flows.

The size of the analysis tile determines the horizontal resolution

3-D Inversion

- RLS (Regularized Least Squares)

$$\chi^2 = \sum_i \frac{1}{\sigma_i^2}\left[U_{x,i} - \iiint d^3x\ K_i(\vec{x})v_x(\vec{x})\right]^2 + \lambda \iiint d^3x\ \left|\vec{\nabla} v_x\right|^2$$

- Employs Three Tile Sizes
  - 2°×2° (22 Mm in diameter)
  - 4°×4° (45 Mm in diameter)
  - 16°×16° (183 Mm in diameter)

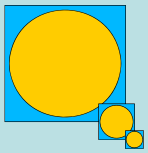

Sensitivity Kernels

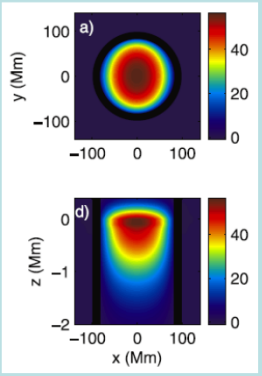

f mode

Horizontal variation of a sensitivity kernel.

The circular shape is determined by the apodization.

Vertical variation of a sensitivity kernel.

The depth dependence is determined by eigenfunctions energy density.

Flows Measured with Local Helioseismology

Large-Scale Flow Maps

Synoptic Flow Map

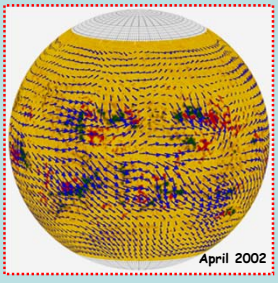

7 Mm below the surface.

Average flow over a month.

The surface differential rotation has been removed.

Flow has been averaged spatially over a scale of ~150 Mm.

Small-Scale Flow Maps

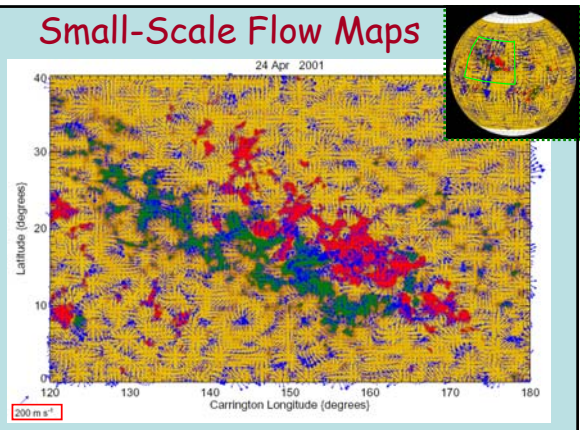

2 degree horizontal resolution

31

Meridional Circulation

By averaging the flows over longitude and many days, the meridional flow can be obtained as function of depth and latitude

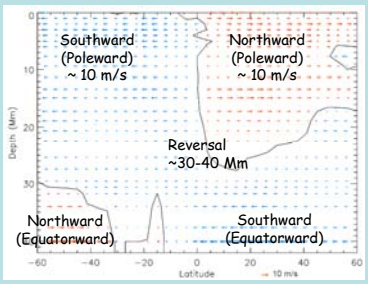

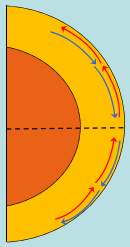

32

Active Regions

Observations from the photosphere and corona

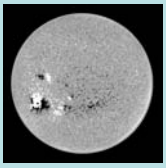

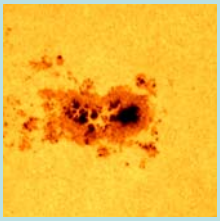

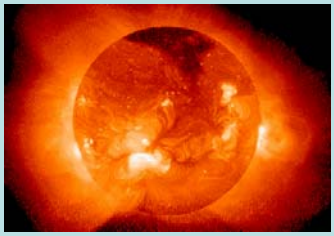

Exploring Subsurface Flows

25 Jan 2002 *11 Jan 2002*

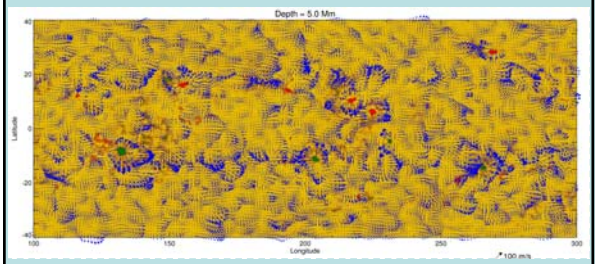

- Multiple-day average over full-disk inversions
- 4 -degree scale most visible at this depth
- Outflows seen around most sunspots at this depth

Spatial Averaged Flows

The fast flows of supergranulation often obscure the slower larger-scale flows. If we look with low resolution a circulation becomes apparent.

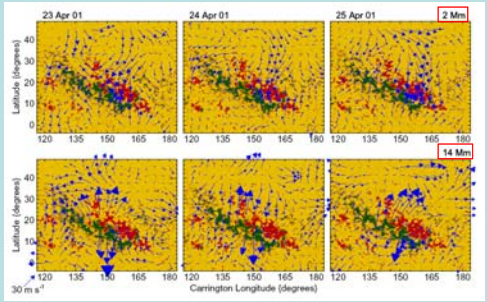

Inflows near the surface

Outflows in deeper layers

35

Schematic Overview

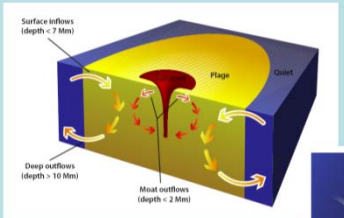

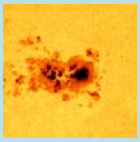

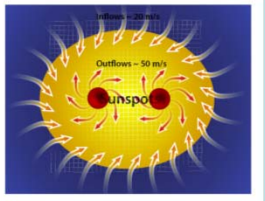

36

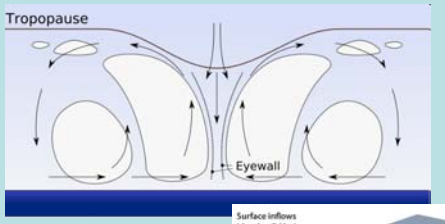

Hurricanes:
Driven by evaporation induced updrafts from a warm sea surface.

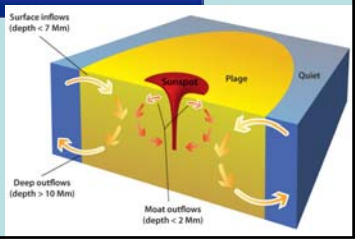

Active Region Circulations:
Driven by cooling induced downdrafts from magnetic plage.

Convection Too!

Of course on top of these large scale circulations, coexist the convection cells due to supergranulation and granulation.

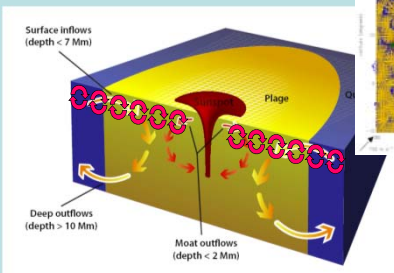

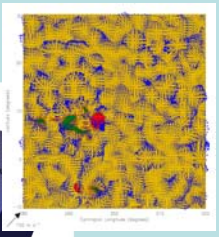

38

Detecting Active Regions
(Before they can be seen at the surface)

39

Detection Prior to Emergence

03:30 UT 26 October 2003

09:30 UT 27 October 2003

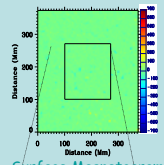

30 hours later

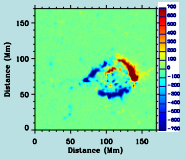

Surface Magnetogram

Active Region NOAA 10488

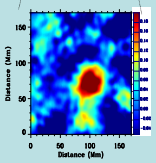

Deep-focus time-distance tomography
Depth 43-75 Mm

6 hours prior to emergence

Time-Distance Tomography

Wave Speed Perturbation Map

Figures courtesy Stathis Ilonidis

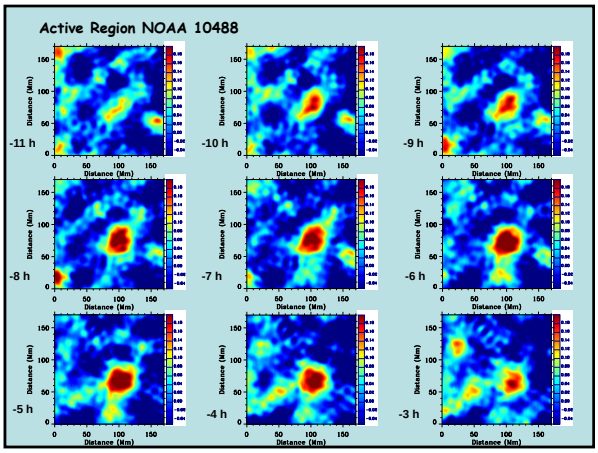

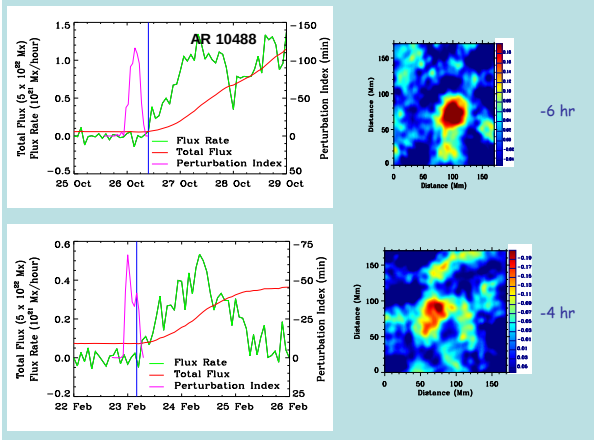

Farside Imaging

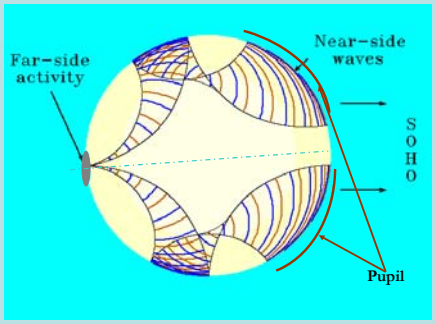

43

Farside Maps

Active Region NOAA-10808

Aug 29 → Sep 9 2005 (GONG)

sin(latitude)

Carrington Longitude

Sept 7 2005

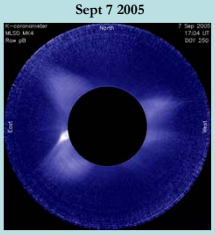

Source: MLSO K-coronameter

Spring 2011

44